 doi:10.20944/preprints201905.0189.v1

Article

Hybrid Analytical Platform Based on Field-Asymmetric Ion Mobility Spectrometry, Infrared Sensing, and Luminescence-Based Oxygen Sensing for Exhaled Breath Analysis

L. Tamina Hagemann, Stefan Repp, Boris Mizaikoff*

Institute of Analytical and Bioanalytical Chemistry (IABC), Ulm University, Albert-Einstein-Allee 11, 89081 Ulm, Germany; boris.mizaikoff@uni-ulm.de.

* Correspondence: boris.mizaikoff@uni-ulm.de; Tel.: +49-731-50-22750

Received: date; Accepted: date; Published: date

Abstract: The reliable online analysis of volatile compounds in exhaled breath remains a challenge as a plethora of molecules occur in different concentration ranges (i.e. ppt to %), and need to be detected against an extremely complex background matrix. While this complexity is commonly addressed by hyphenating a specific analytical technique with appropriate preconcentration and/or preseparation strategies prior to detection, we herein propose the combination of three analytical tools based on truly orthogonal measurement principles as an alternative solution: field-asymmetric ion mobility spectrometry (FAIMS), Fourier-transform infrared (FTIR) spectroscopy-based sensors utilizing substrate-integrated hollow waveguides (iHWG), and luminescence sensing (LS). These three tools have been integrated into a single compact analytical platform suitable for online exhaled breath analysis. The analytical performance of this prototype system was tested via artificial breath samples containing nitrogen (N_2), oxygen (O_2), carbon dioxide (CO_2) and acetone as a model volatile organic compound (VOC) commonly present and detected in breath. Functionality of the combined system was demonstrated by detecting these analytes in their respectively breath-relevant concentration range and mutually independent of each other generating orthogonal yet correlated analytical signals. Finally, adaptation of the system towards the analysis of real breath samples during future studies is discussed.

Keywords: exhaled breath analysis; field-asymmetric ion mobility spectrometry; FAIMS; Fourier-transform infrared spectroscopy; FTIR; luminescence sensing; infrared sensors; hyphenated techniques; hybrid techniques; acetone; carbon dioxide; oxygen

1. Introduction

Breath contains a wide variety of molecules in largely different concentration ranges - from ppt to percent - that are potentially useful for therapy monitoring and elucidation of metabolic pathways. The analysis of such a complex sample by a single analytical techniques is almost impossible. Hence, the combination of orthogonal analytical tools appears to be a viable strategy addressing this issue. To date, predominantly preconcentration, e.g. via solid-phase microextraction (SPME) fibers and needle trap devices (NTD), and/or preseparation schemes, e.g. gas chromatography (GC) or multicapillary (MCC) columns are implemented for addressing trace concentrations, and for reducing the sample complexity. By combining preseparation schemes with FID[1], mass spectrometers, (e.g. TOF-MS[2]) or ion mobility based detectors, e.g. IMS[3] or DMS[4] potent analytical tools have resulted. However, MS-based equipment - while being able to detect a very wide variety of analytes - tends to be costly, bulky and frequently not suitable for online analysis. Also, if only one type of detector is used, potentially useful analytes (i.e. biomarkers) that are not sensitive to the selected detector type remain undetected.

 doi:10.20944/preprints201905.0189.v1

Therefore, the integration of orthogonal detection schemes into a single hybrid analytical platform is the next logical step. Only a few research groups have selected this path for exhaled breath analysis. The probably most commonly selected approach is the use of electronic noses[5–10], i.e. arrays of different colorimetric[8] or metal oxide sensors[9] individually responding to different types of molecules. While these sensors arrays offer portable and rapidly responding breath detection capabilities, specific biomarker identification and inter-device comparability remain challenging[11]. Vaks *et al*.[12] and Shorter *et al*.[13] both combined light sources emitting different wavelengths or even wavelength regimes (i.e. subTHz, THz, IR) in order to broaden the scope of addressable analytes in breath. However, even if these light sources complemented each other, hence providing orthogonality to some extent the basic detection mechanism was essentially similar. Hence, molecules not responding to the respective detection scheme (here, sufficient light absorption in the selected wavelength regimes) will remain undetected. Consequently, truly orthogonal methods are based on different physical principles generating the analytical signals, yet applied to the same sample. This approach has already been proposed[14,15] and put into practice[10,16–20] by various research groups. For example, Covington *et al*.[10] applied an eNose and GC-IMS to the same breath samples, whereas Williams *et al*.[19] parallely used non-dispersive infrared analysis and PTR-TOF-MS on the same sample set. It is important to notice though that all above-mentioned groups except Monks *et al*.[20] applied different analytical methods as standalone-techniques, i.e. the used analytical devices were not integrated into a single setup. This entails extensive sample handling – and potentially associated handling errors – and extended analysis times, e.g. required for separate sample injection and limits application at the patient bedside. Furthermore, with the exception of Williams *et al*.[19] *offline* breath analysis was performed frequently involving gas bags or sample storage, and thus taking the risk of cross-contamination and sample degradation.

Only few groups have developed hybrid analytical devices that enable *online* breath analysis based on truly orthogonal principles integrated in a single sensing platform. Tiele *et al*.[21] published a portable device for CO_2 and O_2 detection that additionally measured temperature and pressure. Miekisch *et al*.[22,23] presented a multidimensional sensing platform including hemodynamic monitoring as well as comprehensive breath monitoring via capnometry, spirometry and PTR-TOF-MS, all being integrated into the same online monitoring platform. While Miekisch *et al*. analyzed human breath, our research team has focused on exhaled mouse breath analysis within a mouse intensive care unit (MICU) at the Institute of Anesthesiologic Pathophysiology and Method Development (IAPMD) at Ulm University Medical Center, which requires as an additional challenge the analysis of exceedingly (i.e. few hundreds of microliters) small breath sample volumes[24–26]. In order to gain metabolic insights, $^{12}CO_2$, $^{13}CO_2$ and O_2 concentrations as well as the respiratory quotient (RQ) were evaluated using various analytical tools (iHWG-FTIR spectroscopy, interband cascade laser based tunable diode laser absorption spectroscopy (TDLAS) and LS), which were all adapted to the challengingly small breath volumes exhaled by a mouse or any comparable small animal model. Besides these already quantifiable analytes in mouse breath, the detection of additional volatile compounds such as acetone and H_2S is currently in development for therapy monitoring and to aid in understanding the underlying metabolism of traumatized mice.

Hence, the present study aims at extending the scope of addressable analytes in mouse breath beyond CO_2 and O_2 by combining FTIR and LS with FAIMS serving as truly orthogonal analytical methods. The detection principles of iHWG based FTIR spectroscopy[27], LS[28] and FAIMS[29] have been described in detail elsewhere. O_2 detection via LS was necessary, as O_2 is neither IR active nor does it give rise to a FAIMS signal. Furthermore, CO_2 could not have been detected by the luminescence sensor and is not ionizable by the ^{63}Ni FAIMS ionization source, and hence, not detectable by FAIMS. In turn, it provides a signal via IR spectroscopy/sensing techniques. Last but not least, the luminescence sensor does not respond to VOCs, and the sensitivity of the selected IR approach would not have allowed for VOC detection at the breath-relevant ppt or ppb concentration range, even though a wide variety of breath-relevant VOCs are IR-active. Hence, integrating FAIMS into the diagnostic platform was essential for reliable and sensitive trace VOC detection.

 doi:10.20944/preprints201905.0189.v1

Synthetic breath samples containing N_2, O_2, CO_2 and acetone as an exemplary breath VOC were prepared and analyzed to demonstrate functionality of the developed hybrid prototype. The presented data proves the feasibility of the integration of FAIMS, FTIR and LS into a single analytical platform for simultaneous online analysis of O_2, CO_2 and acetone as a breath VOC representative. It was shown that the detection of all analytes was possible in the respective breath-relevant concentration range, and that FAIMS, FTIR and LS signals were independent of one another, yet correlated as determined at the same time within the same sample.

2. Materials and Methods

2.1 Hybrid Analytical Platform

2.1.1 Gas Sample Preparation

A stock gas mixture of 2.33 ppm acetone in synthetic air (± 0.23 ppm, MTI Industriegase, Neu-Ulm, Germany) was diluted down by synthetic air (produced with 20.5 vol.% O_2 grade 5.0, remains N_2 grade 5.0, $H_2O \leq 5$ ppmv, $NO+NO_2 \leq 0.1$ ppmv, low molecular weight hydrocarbons $C_nH_m <$ 0.1 ppmv, by MTI Industriegase, Neu-Ulm, Germany) and CO_2 (technical grade (DIN EN ISO 14175), ≥ 99.8 vol-%, $N_2 \leq 1000$ ppmv, $H_2O \leq 120$ ppmv, MTI Industriegase, Neu-Ulm, Germany) to eight samples, containing acetone concentrations between 0 and 20 ppb and a background concentration of 3, 4 or 5 % CO_2 and 19.6 ± 0.5 % O_2 (concentrations given here are volumetric concentrations). The acetone, air and CO_2 flow were regulated by mass flow controllers (Bronkhorst El Flow Prestige, FG-201CV-RBD-11-K-DA-000, 80 mL/min full scale capactiy for acetone; FG-201CV-ABD-11-V-DA-000, 3000 mL/min full scale capacity for synthetic air; Vögtlin red-y smart series, type GSC-A9KS-BB22, 200 mL/min full scale capacity for CO_2). For cleaning and drying purposes, air and CO_2 were filtered through active charcoal (# 20626, Restek, Bad Homburg, Germany), molecular sieve (5Å pore size, # 8475.2, Carl Roth GmbH & Co KG, Karlsruhe, Germany) and sintered glass filter elements (VitraPor®, 40-100 µm, 4-5.5 µm, 1.5 µm). The dew point of air and CO_2 was measured to be -39.8°C (humidity sensor SF52-2-X-T1-B, Michell Instruments, Ely, UK), corresponding to a water content of 192 ppm. The acetone sample gas was neither VOC filtered nor dried, since this would have caused analyte loss. The water content in the acetone gas cylinder was assumed to be negligible due to the dilution of acetone sample gas in comparatively big volumes of CO_2/air.

Acetone and CO_2 were mixed first, by leading their flow through a filter with 0.5 µm pore size (SS-2TF-05, Swagelok, Reutlingen, Germany) to induce turbulences for homogeneous mixing. The combined acetone/CO_2 flow was then combined with the air flow. A schematic of the gas mixing unit is displayed in Figure 1 (left half) in section 2.1.2 together with the hybrid FAIMS-FTIR-LS sensing platform.

2.1.2 Hybrid FAIMS-FTIR-LS Platform and Concentration-Dependent Measurements

The hybrid analytical platform is displayed in Figure 1. Gas samples were provided by the gas mixing unit displayed in the left half of Figure 1 and described in the previous section. The sample flow produced by the gas mixing unit was constantly kept at 2200 mL/min. The relief valve (SS-RL3S4, Swagelok, Reutlingen, Germany) between the gas mixing unit and the FTIR/O_2 sensor unit was adjusted so that the flow reaching the FTIR/O_2 sensor unit was 400 ± 10 mL/min and the flow through the FAIMS PAD was 1800 ± 30 mL/min. These flows were regularly checked on with a digital flow meter (ADM1000, J&W Scientific, Folsom, CA, USA) at the outlet of the O_2 sensor and with the flow sensor integrated in the FAIMS PAD, respectively. To minimize analyte adsorption along the tubing walls, perfluoroalkoxy alkane (PFA) tubings (1/8'' and 1/4'' outer diameter, Swagelok, Reutlingen, Germany) and heated (41 °C) Sulfinert tubings (#29242, Restek, Bad Homburg, Germany) were used in order to minimize analyte adsorption.

Preprints (www.preprints.org) | NOT PEER-REVIEWED | Posted: 15 May 2019 doi:10.20944/preprints201905.0189.v1

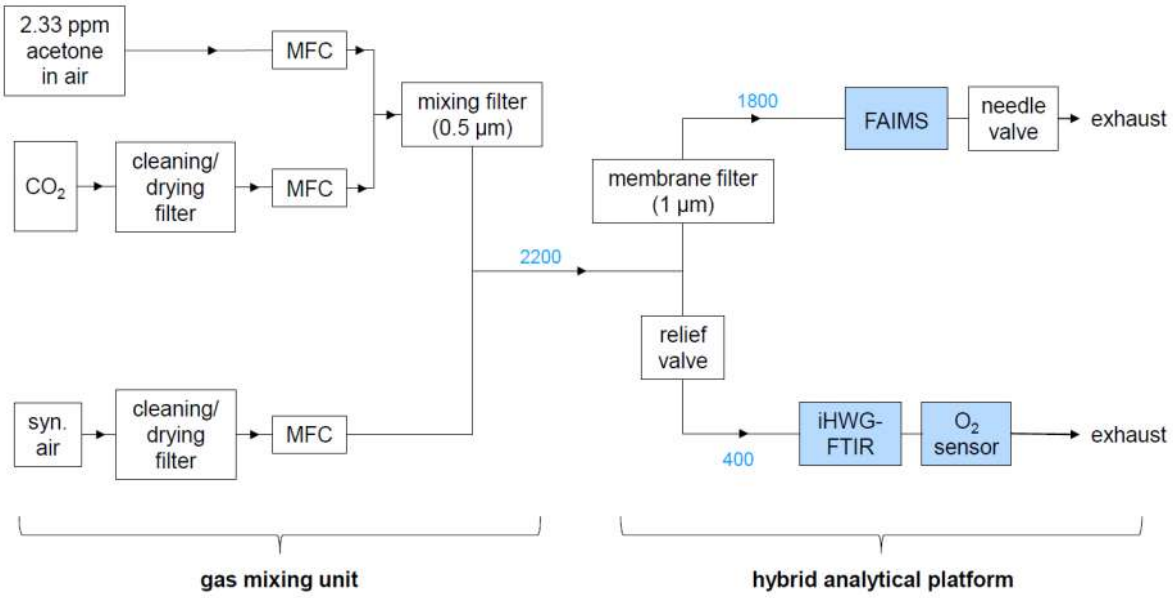

Figure 1. Experimental setup comprising the gas mixing unit and the hybrid analytical platform. Numbers in blue are gas flows in mL/min.

Before starting a measurement series, a hold time was adopted until flow and pressure had stabilized in the FAIMS device (1800 ± 30 mL/min, 0.800 ± 0.020 bar*g*) to ensure reproducibility of the FAIMS data. In case the flow and pressure varied beyond the given limits, the needle valve at the exhaust of the FAIMS as well as the relief valve between FAIMS and FTIR were adjusted until flow and pressure had stabilized for at least ten minutes in the range defined above.

Each measurement series included eight acetone/CO_2/air gas samples. Prior to the analysis of an acetone/CO_2/air mixture, one sample containing pure air and one sample containing only air *and* CO_2 were recorded (see Table 1). During the pure air sample, the FTIR background was recorded, and the according FAIMS spectrum was used to ensure that the system had entirely cleaned down after the previous sample. The CO_2/air measurement, on the other hand, served as a background spectrum for FAIMS. Before analysis, the respective sample gas was led through the setup for at least two minutes to ensure a constant analyte concentration in the whole setup and during the entire measurement.

Table 1: Overview on the measurement protocol within the hybrid setup.

order	injected sample	FAIMS	iHWG-FTIR	LS
1	pure air	verifying system cleanliness	background recording	-
2	CO_2/air	background recording	-	-
3	acetone/CO_2/air	acetone signal recording	CO_2 signal recording	O_2 signal recording
4	repeated for all further samples of a measurement series in random order			

After recording a blank as the first sample of every measurement series, the remaining samples were analyzed in a random sample order that was different in each measurement series. The CO_2 concentration was constant (3, 4 or 5 %) within one measurement series. Three measurement series were recorded per CO_2 concentration. For all air, CO_2/air and all acetone/CO_2/air samples, five FAIMS spectra (~19 min) and five FTIR spectra (~ 3.5 min) were successively recorded, while the sample was continuously flowing through the hybrid setup. Simultaneously, the O_2 concentration was continuously monitored for the duration of the FAIMS measurements.

 doi:10.20944/preprints201905.0189.v1

2.2 Details on the Individual Analytical Methods

2.2.1 Field-Asymmetric Ion Mobility Spectrometry

FAIMS data were recorded with an OEM FAIMS PAD (Owlstone Inc., Cambridge, UK), using the Lonestar software (version 4.912, Owlstone Inc., Cambridge, UK). After ionization by a ^{63}Ni ionization source, analytes were detected by the FAIMS sensor (gap size 37 µm; RF waveform: 267 ± 2 V maximum peak-to-peak voltage, 26 MHz ± 26 Hz RF, 25 % Duty Cycle, 51 steps; compensation voltage (CV) from -6 to +6 V (512 steps, ~4.5 s per full CV scan), flow 1800 ± 30 mL/min; sensor temperature: 60 °C). The sample gas was continuously flowing through the spectrometer at 1800 ± 30 mL/min as the data were recorded. The pressure could be regulated via the needle valve (SS-2MG-MH, Swagelok, Reutlingen, Germany) at the FAIMS outlet and was set to 0.800 ± 0.020 bar*g*. A membrane filter at the inlet of the FAIMS device (polytetrafluoroethylene (PTFE) membrane, 1 µm pore size), heated to 100 °C to avoid analyte accumulation in the filter, prevented particle introduction into the FAIMS PAD. In order to avoid charge build up, the intersweep delay between two subsequent recordings was set to 1500 ms. The obtained FAIMS spectra, also called dispersion plots, displayed the ion current on the detector (z axis) in dependence on the CV (x axis) and the percentage of the dispersion field (DF) which was scanned by varying the peak-to-peak-voltage between 0 and 267 V stepwise.

2.2.2 Substrate-Integrated Hollow Waveguide Coupled Fourier-Transform Infrared Spectroscopy

CO_2 concentrations were monitored via iHWG coupled FTIR spectroscopy. The setup and gas cell have been described in detail elsewhere[30]. Light from an ALPHA FTIR spectrometer (Bruker Optik GmbH, Ettlingen, Germany) was coupled into an iHWG (aluminum, 7.5 cm optical path length, 4x4 mm internal cross-section, produced by fine mechanical workshop West, Ulm University, Ulm, Germany) and then onto the internal detector of the spectrometer via two gold-coated off-axis parabolic mirrors (Thorlabs, MPD254254-90-M01, 2″ RFL). Using the software OPUS (version 7.2, Bruker Optik GmbH, Ettlingen, Germany), IR spectra were recorded in the spectral range from 4000 to 400 cm^{-1} at a spectral resolution of 2 cm^{-1}, with 20 averaged scans, and at a flow rate of 400 ± 10 mL/min. The Fourier transformation was done in OPUS, using the Blackman-Harris 3-term apodization function. In order to exclude CO_2 from ambient air from the optical absorption paths, the entire IR setup was housed in a plastic bag which was purged with synthetic air for at least 15 minutes prior to as well as during each measurement series.

2.2.3 Oxygen Sensing

A flow-through O_2 sensor, detecting O_2 based on luminescence quenching, (FireStingO2, Pyro Science GmbH, Aachen, Germany)[28] was used for monitoring the O_2 concentration, supported by the Software FireSting Logger (version 2.365, PyroScience GmbH, Aachen, Germany). One data point per second was recorded.

2.3 Data Processing

2.3.1 Field-Asymmetric Ion Mobility Spectrometry

Since a direct import of the FAIMS data (.dfm format) into Matlab was not possible, FAIMS data were exported from the Lonestar software as text files and then imported into Matlab (R2018A, The Mathworks Inc., Natick, MA, USA). For baseline correction, the average of the five repetitions of the FAIMS dispersion plot of an CO_2/air sample was substracted from the average of the five repetitions of the subsequent acetone CO_2/air sample. Acetone monomer and dimer peak volumes were approximated by respectively summing all intensity values in selected regions of the dispersion plot (monomer: 68 to 72 % DF, -2.75 to -1.95 V CV; dimer: 46 to 50 % DF, -0.35 to +0.45 V CV). These integration windows were chosen equally wide for monomer and dimer peak and based on a

 doi:10.20944/preprints201905.0189.v1

compromise between achievable signal height and freedom from interferences with other spectral components. The so obtained monomer and dimer peak volumes were then added together to obtain the total acetone signal (from now on, only called "acetone signal"). Singly integrating the monomer *or* the dimer peak would have distorted the FAIMS data evaluation: while the monomer peak was very faint or even invisible at higher acetone concentrations, its contribution to the total acetone signal at higher concentrations would not have been negligible.

After normalization with the mean acetone signal at the maximum measured acetone concentration (20 ppb), the signal was averaged and the standard deviation was calculated. The normalized and averaged acetone signal was plotted against the acetone concentration and an asymptotic fit ($y=A-B\cdot C^x$) was applied. Following IUPAC regulations[31], the concentration at the limit of detection (LOD) and at the limit of quantification (LOQ) was estimated by inserting the signal intensity at the LOD and the LOQ ($\mu_B + 3.29\cdot\sigma_B$ and $\mu_B + 10\cdot\sigma_B$, respectively, with average normalized signal intensity of the blank μ_B and its according standard deviation σ_B) into the inverse of the calibration function ($x=\ln((A-Y)/B)/\ln C$).

2.3.2 Fourier-Transform Infrared Spectroscopy

IR data were imported from OPUS into Origin Pro 2017G. An exemplary spectrum is shown in Figure A1 in the Appendix. For baseline correction, each IR spectrum was shifted by the median of the data set, since the latter suitably represented the baseline. The area under the baseline-corrected IR peak at 2360 cm^{-1} between 2200 and 2450 cm^{-1} was averaged for the five repetitions recorded in a row for each sample. The so obtained CO_2 signal was then normalized by division by the overall maximum CO_2 signal and the normalized signal was averaged for the three repetitions of the measurement series recorded for each CO_2 concentration (3, 4 and 5 % CO_2). The according standard deviation was calculated.

2.3.3 Oxygen Sensing

For each measurement, the O_2 concentrations directly output by the FireSting Logger software was averaged for the time span between 5 and 15 min after starting the O_2 measurement. O_2 concentrations recorded between 0 and 5 min were not included in the average, because the O_2 concentration reached an equilibrium after approximately 5 min (see Figure A2 in the Appendix). The so obtained O_2 signal was then normalized by division by the overall mean O_2 signal; the normalized signal was averaged for the three repetitions of the measurements series recorded for each CO_2 concentration and the standard deviation was calculated.

3. Results and Discussion

3.1 FAIMS Results

As mentioned above, FAIMS dispersion plots of pure air and of CO_2/air were recorded before recording an acetone/CO_2/air containing sample (for further detail also see Table 1 in Section 2.1.2). Figure 2 exemplarily shows a dispersion plot for each sample type collected in positive mode. The dispersion plot of pure air (Figure 2a) mainly showed the reactant ion peak (RIP), which, in positive detection mode, appears due to the formation of ionized clusters of water molecules present in the carrier gas[32]. The faint vertical signal in Figure 2a at around 0 V CV was approximately constant for all recorded dispersion plots. It could not be erased throughout the whole project and was likely to be caused by substances emitted from the tubings and the FAIMS device itself. The CO_2/air dispersion plot (Figure 2b) also mainly showed the RIP. No clear analyte peak appeared, since CO_2 is not ionizable by the ^{63}Ni source. The faint additional trace at around -65 % DF and -3 V CV assumably occurred because of contaminations from the CO_2 gas bottle that could not be entirely removed by the used filters. The acetone/CO_2/air dispersion plot (Figure 2c) showed an intensity decrease of the RIP as well as the appearance of two main additional peaks. Generally, once an ionizable analyte like acetone is inserted into the FAIMS, one or two water molecules in the ionized

Preprints (www.preprints.org) | NOT PEER-REVIEWED | Posted: 15 May 2019 doi:10.20944/preprints201905.0189.v1

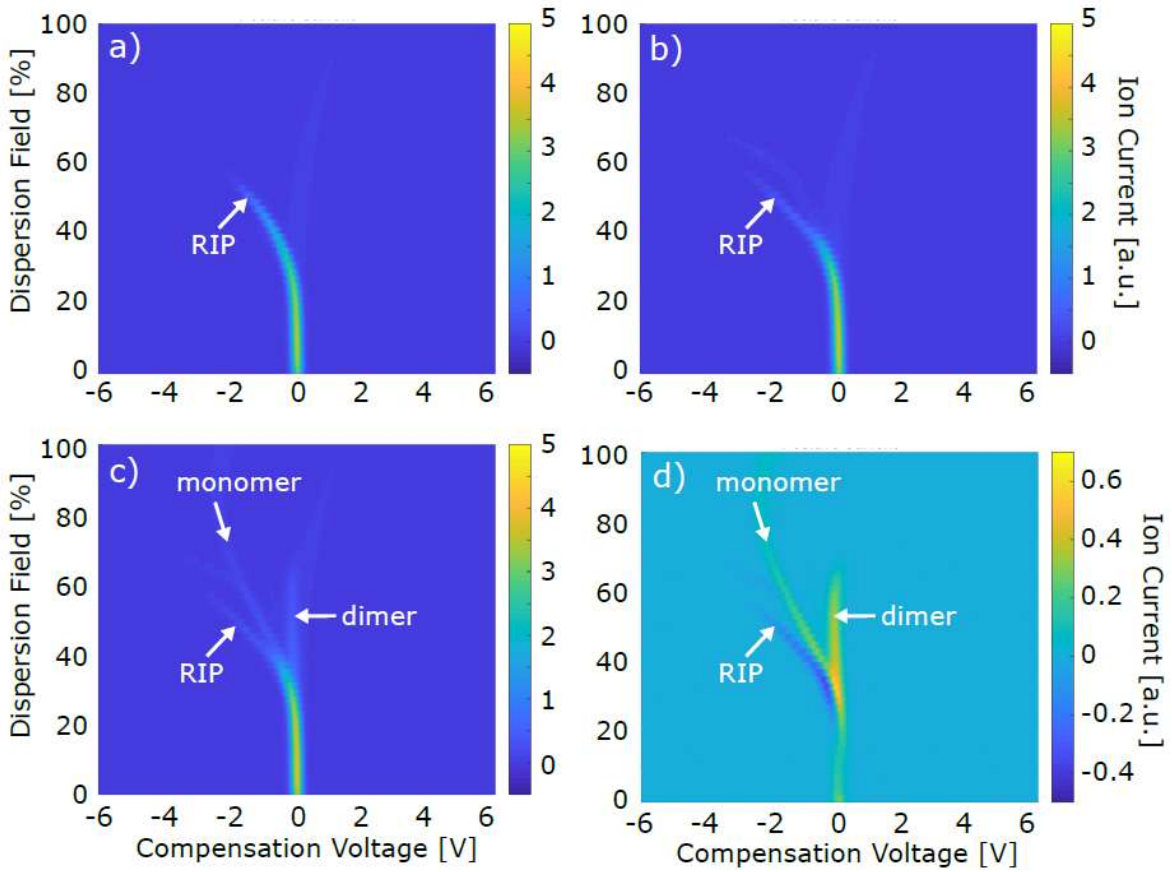

Figure 2. FAIMS dispersion plots. (a) pure air sample (b) CO_2/air sample (c) acetone/CO_2/air sample (d) background substracted acetone/CO_2/air sample ((c) minus (b)). CO_2 and acetone concentration of these exemplary data were 4 % and 1 ppb, respectively. For the sake of clarity, not all four graphs wear all three axes labels.

carrier gas clusters are replaced by the analyte molecules. Hence, the RIP intensity decreases and a monomer and/or dimer peak appear, respectively. The tentative assignment of monomer and dimer peak, as it is indicated in Figure 2c, was based on the concentration-dependent behavior of both peaks: while the monomer peak intensity showed an intensity maximum at lower concentrations, the dimer peak constantly increased with increasing acetone concentration, as an additional water molecule in each monomer cluster was replaced by a second acetone molecule, thus forming a dimer cluster. The relative position of monomer and dimer peak also was in accordance with our expectations and thus substantiated our peak assignment: the lighter, less bulky and hence more mobile monomer cluster gave rise to a peak at a lower CV than the less mobile dimer cluster. The exact origin of the faint feature between monomer and dimer peak in Figures 2c and 2d (~50 %DF, -0.5 V CV) is unknown, but its potential effect is commented on in section 3.2. In order to obtain the net monomer and dimer signal, Figure 2b was subtracted from Figure 2c for background substraction. The resulting data is shown in Figure 2d. The z axis of Figure 2d was varied compared to Figures 2a to 2c in order to make the monomer and dimer peak more clearly visible. At the position where the RIP appeared in Figure 2a to 2c, the signal intensity was negative in Figure 2d, since the RIP intensity decreased while acetone was present in the FAIMS sensing region.

Preprints (www.preprints.org) | NOT PEER-REVIEWED | Posted: 15 May 2019 doi:10.20944/preprints201905.0189.v1

3.2 Co-Dependencies of Acetone, CO_2 and O_2 Signal

The normalized total acetone signal, composed of monomer and dimer peak volume, was plotted against the acetone concentration, shown for 3, 4 and 5 % CO_2 in Figure 3a. Due to saturation of the FAIMS detector, the acetone signal converged towards a maximum value for higher acetone concentrations. Thus, an asymptotic fit was applied. It is obvious from Figure 3a, that the acetone

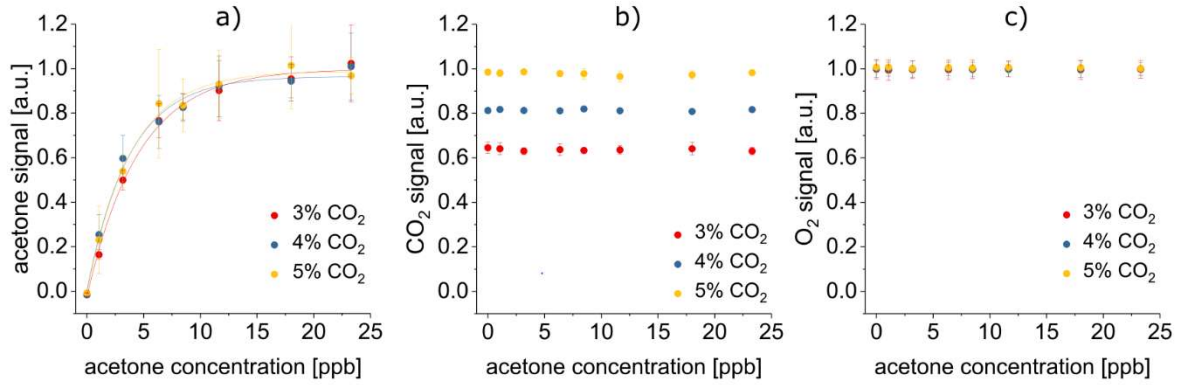

Figure 3: No mutual signal co-dependencies of acetone, CO_2 and O_2 were detected. All displayed error bars are 1σ error bars. (a) Acetone signals recorded with FAIMS depend on the acetone concentration (asymptotic fit $y = A - B \cdot C^x$), yet is independent of the CO_2 content. (b) CO_2 signals recorded by iHWG-FTIR only vary depending on the CO_2 concentration. (c) O_2 signals recorded by LS are neither influenced by the acetone nor by the CO_2 content.

signal was statistically identical, regardless if the CO_2 concentration was 3, 4 or 5 %. Likewise, the according analytical figures of merit, i.e. LOD, LOQ, R^2 and parameters of the asymptotic fit, did not depend on the CO_2 concentration (see Table 2). Hence, the CO_2 concentration did not have any effect on the FAIMS results. Reversely, Figure 3b and 3c reveal, that the acetone concentration did neither affect the CO_2 nor the O_2 signal. Also, the O_2 signal did not change depending on the CO_2 concentration, but stayed constant irrespective if 3, 4 or 5 % CO_2 were present. In conclusion, no mutual co-dependencies of the acetone, CO_2 and O_2 signal were detected.

Table 2: Analytical figures of merit of the concentration-dependent FAIMS measurements of acetone. No statistical difference between fit parameters A, B and C of the asymptotic fit (equation $y = A - B \cdot C^x$) at 3, 4 or 5 % CO_2. R^2, concentration at LOD and concentration at LOQ varied, yet with no clear trend visible depending on the CO_2 content. This indicates independence of the acetone signal from the CO_2 concentration.

	3 % CO2	**4 % CO2**	**5 % CO2**
fit parameter A	0.998 ± 0.019	0.964 ± 0.025	0.989 ± 0.023
fit parameter B	1.024 ± 0.025	0.962 ± 0.038	0.997 ± 0.034
fit parameter C	0.803 ± 0.012	0.765 ± 0.022	0.772 ± 0.019
R^2 >	0.995	0.989	0.992
LOD [ppt]	145	78	56
LOQ [ppt]	358	405	165

The FAIMS error bars shown in Figure 3a are relatively big compared to the FTIR and LS error bars in Figures 3b and 3c, respectively. Several different sources have presumably contributed to the acetone signal variance. First, three slight features apart from RIP, monomer and dimer peak were visible in the dispersion plots of the acetone/CO_2/air sample (see Figure 3c at ~65 % DF / -3 V CV, at ~50 % DF / -0.5 V CV and at ~75 % DF / +0.5 V CV). As mentioned before, these possibly appeared due to contaminations from the CO_2 gas bottle and due to evaporations from the tubings and the FAIMS itself. Even if they do not seem to have fundamentally impacted the obtained data, these contaminations might still have competed with acetone for the ionization energy in the FAIMS

 doi:10.20944/preprints201905.0189.v1

ionization region, therefore possibly altering the acetone signal intensity and increasing the associated error bars. Furthermore, it cannot be excluded that slight humidity variations occured, additionally enhancing the variance of the acetone signal. Finally, the saturation of the FAIMS detector at higher acetone concentrations can be assumed to also have made a contribution to the signal variance.

3.3 Towards Real Breath Analysis

It is our goal to further develop the hybrid FAIMS-FTIR-LS platform towards online analysis of mouse breath. Already with the current setup, the detection of the main breath components CO_2, O_2 and acetone, as a breath VOC representative, was possible in breath-relevant concentrations. Especially the fact that breath VOC detection is possible down to LODs and LOQs in the low to medium ppt range with this hybrid setup, makes it a promising tool for real breath analysis, since breath VOCs most often occur in ppt to ppb concentrations[33]. Furthermore, O_2, CO_2 and acetone signal were found to be mutually independent. This underlines the excellent orthogonality of FAIMS, FTIR spectroscopy and LS, making their combination especially suitable for a complex matrix like exhaled breath: simply by selecting a suitable combination of analytical methods, a first – at least virtual – "preseparation" of the sample components has been undertaken, thus already simplifying the analytical task.

Nevertheless, the hybrid setup and the experiments conducted with it need to be further evolved before online analysis of real mouse breath is possible. First, unlike in our model samples, of course more than one VOC is present in real breath. All these breath VOCs will compete for the FAIMS ionization energy and therefore cause co-dependencies of their signals. To prevent this, preseparation based on a GC or an MCC column will be integrated into the hybrid setup, enabling the VOCs to reach the ionization region one by one. Since the contaminations discussed above (see Figure 2c) will also be separated from the analytes via the GC or MCC column, the FAIMS signal variance may additionally benefit from the preseparation scheme. Furthermore, alkanes, as an important class of breath VOCs[34], cannot be detected with the current setup, because they are not ionized by the ^{63}Ni ionization source. This problem could be overcome by taking advantage of the modular flexibility of the FTIR detection unit: extending the optical path length of the iHWG and replacing the FTIR spectrometer by a more intense light source like a tunable quantum cascade laser, the LOD/LOQ for alkane detection via FTIR could be shifted to breath-relevant concentrations. Moreover, the samples tested until now only contained minimal amounts of water, whereas real breath is oversaturated with humidity. Since the FAIMS detection mechanism is based on ionized water clusters, changes in humidity have a major effect on the FAIMS signal intensity. Here, chemometric data treatment in dependence of the present water level or experimentally filtering out the humidity by a condenser as proposed by Maiti *et al.*[35], which is explicitly suitable for dehumidifying breath without significant VOC loss, could be possible solutions.

4. Conclusions

A compact hybrid sensing platform enabling orthogonal analysis of gas/vapor phase samples based on FAIMS, FTIR and LS was presented, and its utility online analysis of synthetic breath samples containing acetone, CO_2 and O_2 was demonstrated. It was shown that the signals of these compounds were independent of one another, and that all three components could be detected at their respective breath-relevant concentrations. The LOQ of acetone could even be lowered to the medium ppt concentration range, which renders the method a promising approach for the potential analysis of trace level breath VOCs. Yet, challenges according to nonetheless integrating additional analyte preconcentration/-separation strategies and dealing with high humidity levels will need to be resolved prior to the useful analysis of real-world exhaled breath samples, and will be addressed during future studies.

Abbreviations: Å Angström, bar*g* unit for gauge pressure in bar (pressure in bar exceeding atmospheric pressure), CO_2 carbon dioxide, CV compensation voltage, DF dispersion field, FAIMS field-asymmetric ion

 doi:10.20944/preprints201905.0189.v1

mobility spectrometry, FTIR Fourier-transform infrared spectroscopy, GC gas chromatography, IABC Institute for Analytical and Bioanalytical Chemistry, IAPMD Institute for Anesthesiological Pathophysiology and Method Development, iHWG substrate-integrated hollow waveguide, min minutes, LS luminescence sensing, MCC multicapillary column, µL microliter, MICU mouse intensive care unit, N_2 nitrogen, O_2 oxygen, OEM original equipment manufacturer, PFA perfluoroalkoxy alkane, ppb parts per billion, ppm parts per million, ppt parts per trillion, PTFE polytetrafluoroethylene, RIP reactant ion peak, RQ respiratory quotient, TDLAS tunable diode laser absorption spectroscopy, THz Terahertz, VOC volatile organic compound, °C degree Celsius.

Acknowledgments: This work was supported by the Research training group PULMOSENS at Ulm University (GRK 2203) and by the German National Academic Foundation (Studienstiftung des Deutschen Volkes).

Author Contributions: Conceptualization: B.M., L.T.H.; Design, establishment and optimization of setup: L.T.H.; Design of experiment: L.T.H.; Final data acquisition: S.R.; Data evaluation: S.R., L.T.H.; Writing original draft: L.T.H.; Writing-review and editing: B.M., S.R.; Funding acquisition: B.M., L.T.H.; All authors read and approved the final manuscript.

Conflicts of Interest: The authors declare no conflict of interest. The founding sponsors had no role in the design of the study; in the collection, analyses, or interpretation of data; in the writing of the manuscript, and in the decision to publish the results.

Appendix

The primary signals of CO_2 and O_2 recorded by FTIR spectroscopy and LS, respectively, are shown in Figure A1 and A2.

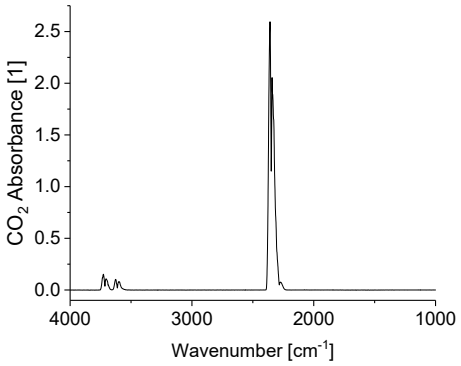

Figure A1: IR spectrum of 4 % CO_2. Acetone theoretically also is IR active, but is not detected here due to its extremely low concentrations in the ppb range.

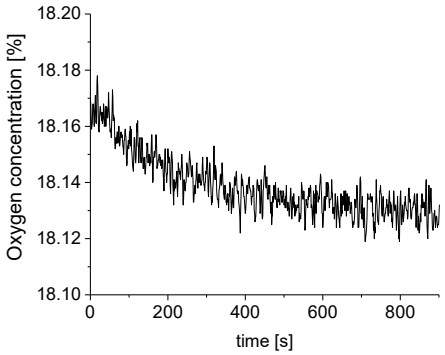

Figure A2: O_2 concentration as detected by the luminescence sensor.

References

1. Mueller, W.; Schubert, J.; Benzing, A.; Geiger, K. Method for analysis of exhaled air by microwave energy desorption coupled with gas chromatography-flame ionization detection-mass spectrometry. *J. Chromatogr. B Biomed. Appl.* **1998**, *716*, 27–38.

2. Smolinska, A.; Klaassen, E.M.M.; Dallinga, J.W.; Van De Kant, K.D.G.; Jobsis, Q.; Moonen, E.J.C.; Van Schayck, O.C.P.; Dompeling, E.; Van Schooten, F.J. Profiling of volatile organic compounds in exhaled breath as a strategy to find early predictive signatures of asthma in children. *PLoS One* **2014**, *9*, e95668.
3. Hüppe, T.; Lorenz, D.; Maurer, F.; Albrecht, F.W.; Schnauber, K.; Wolf, B.; Sessler, D.I.; Volk, T.; Fink, T.; Kreuer, S. Exhalation of volatile organic compounds during hemorrhagic shock and reperfusion in rats: An exploratory trial. *J. Breath Res.* **2016**, *10*, 16016.
4. Basanta, M.; Koimtzis, T. Sampling and analysis of exhaled breath on human subjects with thermal desorption- gas chromatography- differential mobility spectrometry. *Int. J. Ion Mobil. Spectrom.* **2006**, *9*, 45–49.
5. Di Natale, C.; Macagnano, A.; Martinelli, E.; Paolesse, R.; D'Arcangelo, G.; Roscioni, C.; Finazzi-Agrò, A.; D'Amico, A. Lung cancer identification by the analysis of breath by means of an array of non-selective gas sensors. *Biosens. Bioelectron.* **2003**, *18*, 1209–1218.
6. Machado, R.F.; Laskowski, D.; Deffenderfer, O.; Burch, T.; Zheng, S.; Mazzone, P.J.; Mekhail, T.; Jennings, C.; Stoller, J.K.; Pyle, J.; et al. Detection of lung cancer by sensor array analyses of exhaled breath. *Am. J. Respir. Crit. Care Med.* **2005**, *171*, 1286–1291.
7. Peng, G.; Tisch, U.; Adams, O.; Hakim, M.; Shehada, N.; Broza, Y.Y.; Billan, S.; Abdah-Bortnyak, R.; Kuten, A.; Haick, H. Diagnosing lung cancer in exhaled breath using gold nanoparticles. *Nat. Nanotechnol.* **2009**, *4*, 669–673.
8. Mazzone, P.J.; Wang, X.F.; Xu, Y.; Mekhail, T.; Beukemann, M.C.; Na, J.; Kemling, J.W.; Suslick, K.S.; Sasidhar, M. Exhaled Breath Analysis with a Colorimetric Sensor Array for the Identification and Characterization of Lung Cancer. *J. Thorac. Oncol.* **2012**, *7*, 137–142.
9. De Vries, R.; Brinkman, P.; Van Der Schee, M.P.; Fens, N.; Dijkers, E.; Bootsma, S.K.; De Jongh, F.H.C.; Sterk, P.J. Integration of electronic nose technology with spirometry: Validation of a new approach for exhaled breath analysis. *J. Breath Res.* **2015**, *9*, 46001.
10. Tiele, A.; Wicaksono, A.; Kansara, J.; Arasaradnam, R.P. Breath Analysis Using eNose and Ion Mobility Technology to Diagnose Inflammatory Bowel Disease — A Pilot Study. *Biosensors* **2019**, *9*, 55–70.
11. Fens, N.; van der Schee, M.P.; Brinkman, P.; Sterk, P.J. Exhaled breath analysis by electronic nose in airways disease. Established issues and key questions. *Clin. Exp. Allergy* **2013**, *43*, 705–715.
12. Vaks, V.L.; Domracheva, E.G.; Pripolzin, S.I.; Chernyaeva, M.B. Multifrequency high precise subTHz-THz-IR spectroscopy for exhaled breath research. *Terahertz Emit. Receiv. Appl. VII* **2016**, *9934*, 99340E–1 to 99340E–10.
13. Shorter, J.H.; Nelson, D.D.; McManus, J.B.; Zahniser, M.S.; Milton, D.K. Multicomponent Breath Analysis With Infrared Absorption Using Room-Temperature Quantum Cascade Lasers. *NIH Public Access* **2010**, *10*, 76–84.
14. Ibrahim, W.; Wilde, M.; Cordell, R.; Salman, D.; Ruszkiewicz, D.; Bryant, L.; Richardson, M.; Free, R.C.; Zhao, B.; Yousuf, A.; et al. Assessment of breath volatile organic compounds in acute cardiorespiratory breathlessness: A protocol describing a prospective real-world observational study. *BMJ Open* **2019**, *9*, 1–13.
15. Inside the Breath Cluster https://www.insidebreath.com/en/, accessed on April 30th 2019.
16. Dharmawardana, N.; Ooi, E.; Goddard, T.; Woods, C.; Watson, D.; Yazbek, R. Characterization of breath volatile organic compounds in patients with upper aerodigestive mucosal squamous cell carcinoma. *IABR Breath Summit* 2018.
17. Gould, O.; Ratcliffe, N.; de Lacy, C.B.; Francis, N.; Young, N. Approaches to a simple breath test for the

early diagnosis of post-operative complications following colorectal cancer and segmental resection. *IABR Breath Summit* 2018.

18. Shimouchi, A.; Jinno, N.; Taniguchi, K.; Okumura, N.; Miyamoto, Y. Volatile compounds in exhaled air associated with scores of general physical and mental conditions. *IABR Breath Summit* 2018.
19. Williams, J.; Stönner, C.; Wicker, J.; Krauter, N.; Derstroff, B.; Bourtsoukidis, E.; Klüpfel, T.; Kramer, S. Cinema audiences reproducibly vary the chemical composition of air during films, by broadcasting scene specific emissions on breath. *Sci. Rep.* **2016**, *6*, 1–10.
20. Wilde, M.J.; Cordell, R.L.; Salman, D.; Zhao, B.; Ibrahim, W.; Bryant, L.; Ruszkiewicz, D.; Singapuri, A.; Free, R.C.; Gaillard, E.A.; et al. Breath analysis by two-dimensional gas chromatography with dual flame ionisation and mass spectrometric detection – method optimisation and integration within a large-scale clinical study. *J. Chromatogr. A* **2019**, *1594*, 160–172.
21. Tiele, A.; Covington, J. Design and development of an end-tidal breath capture device. *IABR Breath Summit* 2018.
22. Sukul, P.; Trefz, P.; Kamysek, S.; Schubert, J.K.; Miekisch, W. Instant effects of changing body positions on compositions of exhaled breath. *J. Breath Res.* **2015**, *9*, 47105.
23. Sukul, P.; Schubert, J.K.; Kamysek, S.; Trefz, P.; Miekisch, W. Applied upper-airway resistance instantly affects breath components: A unique insight into pulmonary medicine. *J. Breath Res.* **2017**, *11*, 47108.
24. Fortes, P.R.; Wilk, A.; Seichter, F.; Cajlakovic, M.; Koestler, S.; Ribitsch, V.; Wachter, U.; Vogt, J.; Radermacher, P.; Carter, C.; et al. Combined sensing platform for advanced diagnostics in exhaled mouse breath. *Front. Biol. Detect. From Nanosensors to Syst. V* **2013**, *8570*, 85700Q–1 to 85700Q–9.
25. Seichter, F.; Tütüncü, E.; Hagemann, L.T.; Vogt, J.; Wachter, U.; Gröger, M.; Kress, S.; Radermacher, P.; Mizaikoff, B. Online monitoring of carbon dioxide and oxygen in exhaled mouse breath via substrate-integrated hollow waveguide Fourier-transform infrared- luminescence spectroscopy. *J. Breath Res.* **2018**, *12*, 036018.
26. Tütüncü, E.; Nägele, M.; Becker, S.; Fischer, M.; Koeth, J.; Wolf, C.; Köstler, S.; Ribitsch, V.; Teuber, A.; Gröger, M.; et al. Advanced Photonic Sensors Based on Interband Cascade Lasers for Real-Time Mouse Breath Analysis. *ACS Sensors* **2018**, *3*, 1743–1749.
27. Wilk, A.; Chance Carter, J.; Chrisp, M.; Manuel, A.M.; Mirkarimi, P.; Alameda, J.B.; Mizaikoff, B. Substrate-integrated hollow waveguides: A new level of integration in mid-infrared gas sensing. *Anal. Chem.* **2013**, *85*, 11205–11210.
28. Seichter, F.; Vogt, J.; Radermacher, P.; Mizaikoff, B. Nonlinear calibration transfer based on hierarchical Bayesian models and Lagrange Multipliers: Error bounds of estimates via Monte Carlo – Markov Chain sampling. *Anal. Chim. Acta* **2017**, *951*, 32–45.
29. Covington, J.A.; van der Schee, M.P.; Edge, A.S.L.; Boyle, B.; Savage, R.S.; Arasaradnam, R.P. The application of FAIMS gas analysis in medical diagnostics. *Analyst* **2015**, *140*, 6775–6781.
30. Hagemann, L.T.; McCartney, M.M.; Fung, A.G.; Peirano, D.J.; Davis, C.E.; Mizaikoff, B. Portable combination of Fourier transform infrared spectroscopy and differential mobility spectrometry for advanced vapor phase analysis. *Analyst* **2018**, *143*, 5683–5691.
31. Inczédy, A. *IUPAC Compendium of Analytical Nomenclature: Definitve Rules. Chapter 18.4.3.7*; 3rd ed.; 1997;
32. Eiceman, G.A.; Karpas, Z. *Ion Mobility Spectrometry*; 2nd ed.; Taylor & Francis Group LLC: Boca Raton, FL, USA, 2005;
33. Phillips, M. Method for the collection and assay of volatile organic compounds in breath. *Anal. Biochem.* **1997**, *247*, 272–278.

 doi:10.20944/preprints201905.0189.v1

34. Cheepsattayakorn, A.; Cheepsattayakorn, R. Breath tests in respiratory and critical care medicine: From research to practice in current perspectives. *Biomed Res. Int.* **2013**, *2013*, 702896.

35. Maiti, K.S.; Lewton, M.; Fill, E.; Apolonski, A. Sensitive spectroscopic breath analysis by water condensation. *J. Breath Res.* **2018**, *12*, 046003.